Two-Dimensional VIV Simulation of a Cylinder Close to a Wall with High Reynolds Number by Overset Mesh

Li, Ruan
Interdisciplinary Graduate School of Engineering Sciences, Kyushu University

Karma, Mohamed
Research Institute for Applied Mechanics, Kyushu University

Hu, Changhong
Research Institute for Applied Mechanics, Kyushu University

https://doi.org/10.5109/6781072

出版情報：Evergreen. 10 (1), pp.219-229, 2023-03. 九州大学グリーンテクノロジー研究教育センター
バージョン：

Two-Dimensional VIV Simulation of a Cylinder Close to a Wall with High Reynolds Number by Overset Mesh

Ruan Li[1], Mohamed Karma[2], Changhong Hu[2,*]

[1]Interdisciplinary Graduate School of Engineering Sciences, Kyushu University, Japan

[2]Research Institute for Applied Mechanics, Kyushu University, Japan

E-mail: ruanli19910225@gmail.com

(Received November 11, 2022; Revised January 19, 2023; accepted January 21, 2023).

Abstract: The numerical study of vortex-induced vibration (VIV) of a near-wall cylinder, as well as the impacts of the wall on VIV response, is presented. The Reynolds number for a cylinder near a wall is lower than that of an isolated cylinder when the max vibration amplitude occurs. The max vibration amplitude of the cylinder near a wall is less than that of an isolated cylinder. Moreover, the vortex shedding observed from a wall interacts with the vortex shedding emanating from a cylinder, weakening it. As a near-wall cylinder enters the lock-in region, the vortex shedding from a wall interact with that from the cylinder, which promote separation of the wall boundary layer and alter the wake vortex structure.

Keywords: Wall effects; Vortex-induced vibrations; Overset mesh; Vortex shedding;

1. Introduction

Although natural gas and oil are still the main energy sources of the world, new energy sources including offshore wind power are developing all the time. Japanese government carried out policies to accelerated the development of the offshore wind power for confirming energy security[1-3].

Slender subsea structures like cables, pipelines, risers and jumpers when exposed to the current may experience vortex-induced vibrations (VIV), that could reduce structural fatigue life and increase risk of structural failure. The proximity of the sea bottom will change the flow around the cable and its wake. Such current-induced vibrations may cause engineering accidents. Therefore, it is important to study the VIV of a cylinder near a wall.

Because of a wall, the fluid flow mechanism of the cylinder near a wall becomes more complicated compared with those in isolated conditions[4]. Jones and Tsahalis discovered that the track of a cylinder near a wall is an elliptical shape at X and Y direction, instead of the traditional 8 shapes for an isolated cylinder[5]. Fredsøe and Sumer reported that at reduced velocity $U_r < 3$ and gap ratio $G/D > 0.3$, the transverse vibration frequency of the cylinder near a wall is approximate to vortex shedding frequency of a fixed cylinder[6]. While Ur is from 3 to 8, the deviation between the two frequencies is considerable. Yang and Gao discovered a reduction in transverse vibration amplitudes with reducing gap ratio G/D by studying the VIV of a cylinder near a wall in the turbulent regime in an experiment[7]. Yang and Gao discovered experimentally that vibration range increases with reducing mass ratio m*. At the same decreased velocity, the frequency ratio (which is the ratio of transverse vibration frequency to natural frequency of a cylinder) for smaller m* is substantially bigger[8]. Dimensionless vibration frequencies for lower $G/D = 0.06\ and\ 0.30$ are much higher than those for higher $G/D = 0.66\ and\ 0.88$.

MingZhao used 2D RANS equations to explore 2-DoF VIV of a cylinder near a wall, as well as impacts of a plane wall on VIV at the G/D is exceedingly narrow ($G/D = 0.002$)[9]. Wang and Hao experimented a 1-DoF VIV of a cylinder near a wall and found that vibration amplitude and vibration frequency of a cylinder are affected by a wall, which also cause non-linearities response of the cylinder[10]. Tham et al found that when $m^* = 10$ and $R_e = 100$, the initial branch and lower branch in the amplitude curve against reduced velocity Ur at $0.75 < G/D < 10$ are observed, which is similar to an isolated cylinder, and at $G/D = 0.5$, two transverse vibration peak amplitudes could be observed[11]. Li and Yao presented that when $R_e = 200$ and $G/D = 0.9$, a numerical simulation for a cylinder near a wall[12]. They discovered that due to the wall's effect, the mean lift force is increased, the vortex shedding from bottom half of the cylinder is inhibited by both vortex shedding from the top portion of the cylinder and the wall boundary layer[13].

Many experiments and numerical studies are conducted to further understand the dynamic response of VIV of the cylinder near a wall. Previous researches are largely centered on the dynamic response of VIV of a cylinder close to a wall in the laminar flow. In this paper, the dynamic response of VIV of an elastically supported

cylinder for low mass ratio near a wall at high Re in the turbulent regime is numerically investigated based on open-source software OpenFOAM[14-22].

It is well known that the mesh quality is important for the numerical solution. In a numerical simulation with overset mesh, the body motion is simulated depending upon the relative positions of different component meshes and the shape of each component mesh is fixed. Therefore overset mesh could maintain the mesh quality with the large motions of a body, and the mesh quality could be kept regardless of the magnitude of body motions[23-25].

The other parts of this paper are structured as follows. The mathematical model and governing equations are stated in Section 2. Section 3 describes problem definition as well as the mesh independence analysis. Section 4 describes the discussion and the results. Finally, Section 5 highlights the key concluding remarks.

2. Mathematical model

In this paper, a transient solver and Reynolds Averaged Navier-Stokes (RANS) methods are adopted to work out the governing equations of the cylinder and flow motion based on open-source software OpenFOAM. The methods are shown below and the physical quantities are displayed in Table.

2.1 Numerical method and governing equations

The physical quantities about ocean current are shown in Table 1.

Table 1. Physical quantities about ocean current.

Physical quantities	Symbol
The velocity vectors at the *i* direction	u_i
The position vectors at the *i* direction	x_i
The time	t
The pressure	p
The fluid density	ρ
The dynamic viscosity	υ
The strain rate tensor	S_{ij}
The Reynolds stress tensor	$\overline{u_i'u_j'}$
The turbulence kinetic energy	k
The mean flow velocity	U
The turbulence intensity	I
The reference length scale	L
The kinematic eddy viscosity	υ_t
The Kronecker symbol	δ_{ij}

The Navier-Stokes equations and two dimensional continuity equation for incompressible viscous flows are adopted as shown below.

$$\frac{\partial u_i}{\partial x_i} = 0 \tag{1}$$

$$\frac{\partial u_i}{\partial t} + u_j\frac{\partial u_i}{\partial x_j} = -\frac{1}{\rho}\frac{\partial p}{\partial x_i} + \frac{\partial}{\partial x_j}\left(2\upsilon S_{ij} - \overline{u_i'u_j'}\right) \tag{2}$$

The equations of S_{ij} and $\overline{u_i'u_j'}$ are as follows:

$$S_{ij} = \frac{1}{2}\left(\frac{\partial u_i}{\partial x_j} + \frac{\partial u_j}{\partial x_i}\right) \tag{3}$$

$$\overline{u_i'u_j'} = \upsilon_t\left(\frac{\partial u_i}{\partial x_j} + \frac{\partial u_j}{\partial x_i}\right) + \frac{2}{3}k\delta_{ij} \tag{4}$$

It is well known that the unsteady RANS equations are unclosed, it is necessary to incorporate the extra equations, namely a turbulence closure equation. The k-omega Shear Stress Transport (SST *k*-ω) turbulence model is the most generally used model in the industry, and it has already been used in a large number of publications about VIV of the cylinder near a wall; So it was used in this research, and specific model parameter settings are same to the literature[26].

SST *k*-ω is a two-equation model with the turbulence kinetic energy k, and turbulence specific dissipation rate ω. For isotropic turbulence:

$$k = \frac{3}{2}(UI)^2 \tag{5}$$

$$\omega = \frac{k^{0.5}}{C_\mu^{0.25}L} \tag{6}$$

where C_μ is a constant equal to 0.09.

To realistically model a given problem, it is important to define the turbulence intensity at the inlets. In this paper, the incoming turbulence intensity is high turbulence, so the turbulence intensity $I = 0.1U$.

2.2 Motion equation

The physical quantities about cylinder are shown in Table 2.

Table 2. Physical quantities about cylinder.

Physical quantities	Symbol
The diameter	D
The structural mass	m
The added mass	m_a
The structural damping	c
The structural stiffness	k
The displacement in the in-line direction	X
The displacement in the transverse direction	Y
The drag force and drag coefficient	F_D and C_D
The lift force and lift coefficient	F_L and C_L
The mass ratio	m^*
The reduced velocity	U_r

The natural frequency	f_n
The damping ratio	ξ

The 2DOF dynamic equations of the vibration cylinder are shown below:

$$(m + m_a)\ddot{X} + c\dot{X} + kX = F_D \tag{7}$$

$$(m + m_a)\ddot{Y} + c\dot{Y} + kY = F_L \tag{8}$$

The parameters could be nondimensionalized as:

$$x = \frac{X}{D}, \quad y = \frac{Y}{D}, \quad t = \frac{TU}{D},$$
$$m^* = \frac{m}{m_a}, \quad m_a = \frac{\pi\rho D^2}{4}, \quad U_r = \frac{U}{f_n D}, \tag{9}$$
$$k = (m + m_a)(2\pi f_n)^2, \quad \xi = \frac{c}{2\sqrt{k(m + m_a)}}$$
$$F_D = \frac{1}{2}\rho D U^2 C_D, \quad F_L = \frac{1}{2}\rho D U^2 C_L$$

where the nondimensional parameters x, y and t are displacements and time respectively.

Then, the nondimensional motion equations for the vibration cylinder could be written as follow:

$$\ddot{x} + \frac{4\pi\xi}{U_r}\dot{x} + \frac{4\pi^2}{{U_r}^2}x = \frac{2}{\pi m^*}C_D \tag{10}$$

$$\ddot{y} + \frac{4\pi\xi}{U_r}\dot{y} + \frac{4\pi^2}{{U_r}^2}y = \frac{2}{\pi m^*}C_L \tag{11}$$

3. Numerical simulation

3.1 Numerical model

In this paper, the open-source software OpenFOAM is used for 2D numerical simulation of 2DOF VIV of a cylinder close to a wall. The numerical model is depicted in Fig. 1.

As shown in Fig. 1, a cylinder is placed next to a wall, its center is at the origin of the coordinate system and it is 10D aside inlet boundary and 20D aside outlet boundary respectively. Top boundary is placed 10D above the cylinder's center.

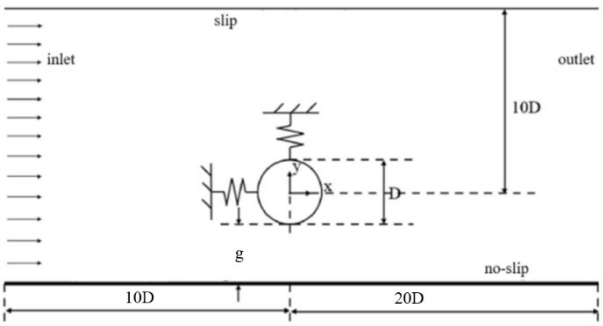

Fig. 1: Schematic diagram.

In the simulation, the no-slip boundary condition is considered for the wall boundary and cylinder surface. A constant and uniform flow is applied at the inlet boundary. A slip boundary condition is used for the top boundary. The zero and zero-gradient are assigned to the pressure and velocity at the outlet boundary, respectively.

Moreover, the wall function is considered for the wall boundary and cylinder surface, when using wall functions approach which can model the near wall region, there is no need to resolve the boundary layer, which yields to a significant reduction of the mesh size and the computational domain. In this paper, the default boundary function which come from OpenFOAM are assigned to turbulent viscosity *nut*, turbulent energy *k*, turbulent dissipation rate ω, respectively. In OpenFOAM these wall functions can provide the accurate result[27].

In this paper, the open-source software OpenFOAM is used to solve the unsteady incompressible RANS equation based on the finite volume method. The time terms are discretized by the first order implicit Euler scheme. The gradient terms are discretized by the Gauss linear scheme. The divergence term of velocity is discretized by the Gauss limitedLinearV 1 scheme and the divergence terms of other parameters are discretized by the Gauss limitedLinear 1 scheme. The terminology 'limitedLinear' stands for that the scheme limits towards upwind in regions of rapidly changing gradient. The coefficient '1' means strongest limiting, and 'V scheme' uses a single limiter which is calculated based on the direction of most rapidly changing gradient, resulting in the strongest limiter being calculated which is most stable. The Laplacian term is discretized by the Gauss linear corrected scheme; The linear interpolation is used, and the solving method is PIMPLE method. All those are standard definitions in OpenFOAM.

In this paper, the gap ratio $g/D = 1$, mass ratio $m^* = 2.6$, damping ratio $m^*\xi = 0.013$, reduced velocity Ur is from $U_r = 3$ to $U_r = 15$, corresponding Re is from $R_e = 15677$ to $R_e = 78387$.

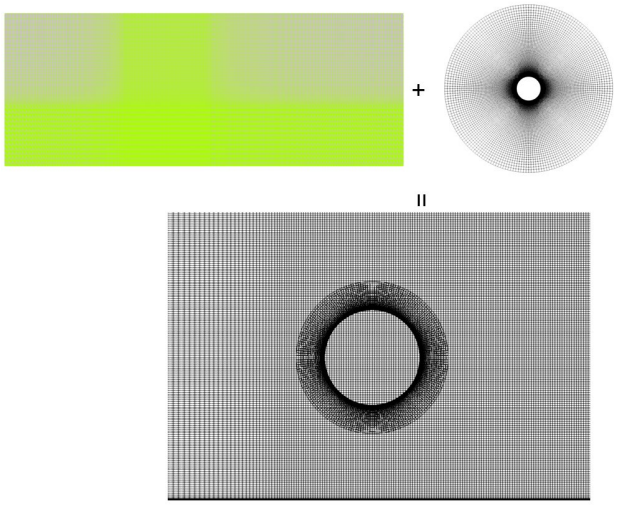

Fig. 2: Schematic diagram of overset mash.

3.2 Overset mesh

Overset meshes, unlike other mesh methods, do not

need mesh deformation or remeshing. The mesh quality is maintained throughout the simulation. This is particularly appealing for large mesh deformation caused by body movements. The numerical solution for this class of problems using overset meshes involves creating two meshes: one fixed background mesh and one moving mesh fitted to the moving body. The domain connectivity is obtained through proper interpolation in the overlapping areas. As shown in Fig. 2, these two overlapping meshes are used.

3.3 Validation

During our literature review for this paper, we discovered that many publications validate their respective numerical models by comparing them to the numerical simulation findings of other authors. As a result, we decided to verify our numerical results using numerical from Naito et al., Singh et al., Tham et al., and Chen et al.

A DNS numerical simulation of flows past a fixed cylinder are conducted to verify the present numerical approach. As shown in Table 3, compared to the results of Naito et al., the present results are largely consistent with those of Naito and Fukagata[28].

Table 3. Comparison for a fixed cylinder

Re = 100	(CD)ave	(CL)rms	St
Present	1.35	0.22	0.165
Reference	1.33	0.23	0.165

Simulations of flows past an isolated cylinder which are the same parameters as those in Singh et al. [29], are also conducted to validate the present numerical approach. As shown in Fig. 3, at the same parameters $m^* = 10$, $\xi = 0$, $R_e = 100$, compared to the results of Singh and Mittal., the present results are largely consistent with those of Singh except when $U_r = 8$.

Because the wall effect is being investigated in this research, further confirmation of the dynamic response of a near-wall cylinder is required. The numerical calculation parameters are identical to those of the VIV system in Refs. 11 and 21. As illustrated in Fig. 4, at the same parameters $m^* = 10$, $\xi = 0$, $R_e = 100$ and the $g/D = 0.5$, present results are compared to these of Refs. 11 and 21 and the present results are largely consistent with literature. Consequently, the numerical model presented in this study is considered to be valid.

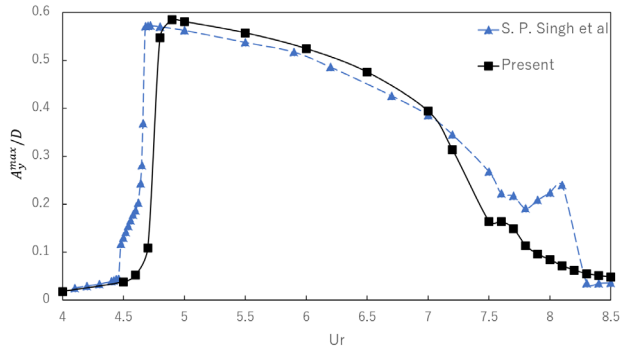

Fig. 3: Comparison with Singh and Mittal for the isolated cylinder.

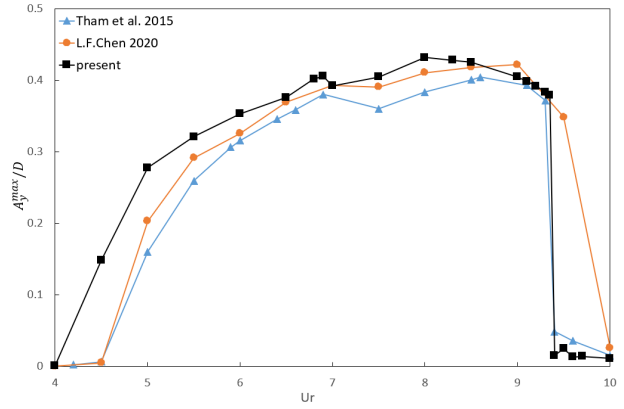

Fig. 4: Comparison of VIV simulation of the cylinder near a wall.

3.4 Mesh independence

The effect of the mesh on the precision of numerical simulation results is investigated in this section. Table 3 shows the results of using five different meshes of various sizes at $m^* = 2.6$, $m^*\xi = 0.013$, $R_e = 36580$, $g/D = 1$ and $U_r = 7$.

As shown in Table 4, the solutions appear to converge when the mesh density is increased. The results obtained with the more rough meshes M1, M2, and M3 are compared to these with the finer meshes M4 and M5. The discrepancies are shown in brackets. As a result, the mesh M4 has been chosen to conduct the following 2D simulations because of its accuracy and computational efficiency.

Table 4. Mesh independence study: the VIV of a cylinder near a wall at $U_r = 7$.

Mesh	Number of elements	(Ay)max/D	(Ax)max/D	(CD)ave	(CL)rms
M1	115600	0.92669 (-2.74%)	0.06092 (-2.71%)	2.01747 (1.27%)	0.45538 (8.21%)
M2	117200	0.95818 (0.57%)	0.06708 (7.12%)	2.08831 (4.83%)	0.48571 (15.42%)
M3	132700	0.95578 (0.32%)	0.06600 (5.40%)	2.08266 (4.54%)	0.48354 (14.90%)
M4	146300	0.95275	0.06262	1.99213	0.42083
M5	158800	0.94999 (-0.29%)	0.06257 (-0.08%)	1.98571 (0.32%)	0.41786 (-0.71%)

4. Results and discussion

The associated physical phenomena become more complex as a cylinder is nearing a wall because of the interactions between cylinder and wall. Because unsteady wake of a near-wall cylinder interacts with the wall, these coupled dynamic responses are unlike an isolated cylinder. In this paper, to explore the coupled dynamic responses in turbulence flow, a cylinder near a wall at a gap ratio $g/D = 1$ is selected, the dynamics response of an isolated cylinder equivalent is compared.

4.1 In-line and transverse amplitudes

As shown in Fig. 5, the nondimensional in-line and transverse max vibration amplitudes of an isolated cylinder and a near-wall cylinder at a gap ratio $g/D = 1$ is described.

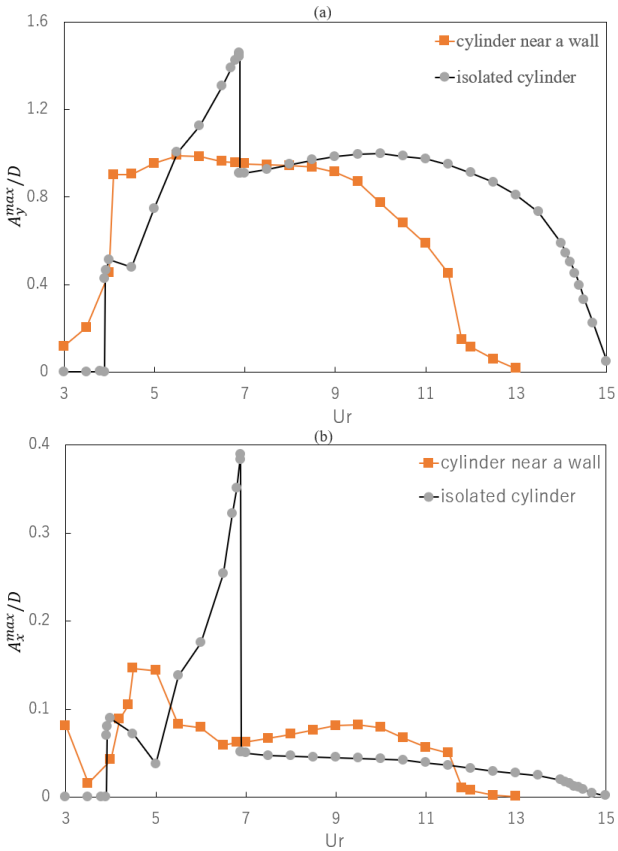

Fig. 5: Max vibration amplitudes: (a) transverse; (b) in-line.

As Ur increases, the cylinder response region is often split into four parts: the initial branch, upper branch, lower branch, desynchronization branch respectively.

As shown in Fig. 5(a), compared to an isolated cylinder, the upper branch and lower branch of a near-wall cylinder are merged into one upper branch, meanwhile the max in-line and transverse vibration amplitude are smaller. At the initial branch ($U_r < 4$), the transverse vibration amplitude of a near-wall cylinder is more than these of an isolated cylinder due to wall effect, it seems that the wall's effect is to increase vibrating rather than decreasing it. Until $U_r > 5.5$ as Ur increases, the effect of the wall will suppress the transverse vibration amplitude. By comparison, as shown in Fig. 5(b), when $7 < U_r < 11.8$, because of the effect of the wall, the in-line vibration amplitude of near-wall cylinder is more than these of an isolated cylinder.

As shown in Fig. 5(a), the existence of wall affects the entire shape of response curve. As Ur enters the pre-lock-in area ($U_r < 4$), the transverse vibration amplitudes of cylinder near a wall are larger than that of an isolated cylinder. When Ur increases up to about 4, the transverse vibration amplitudes both quickly increase, and when $U_r > 5.5$, the transverse vibration amplitudes of a near-wall cylinder becomes smaller. The transverse vibration amplitudes of the isolated cylinder quickly fall off when it jumps down from upper branch to lower branch at $U_r = 6.88$, meantime the transverse vibration amplitudes of a near-wall cylinder drop gradually. As Ur increases further, the near-wall cylinder more quickly leaves the lock-in area when $U_r = 11.8$ while an isolated cylinder leaves the lock-in region at $U_r = 14$.

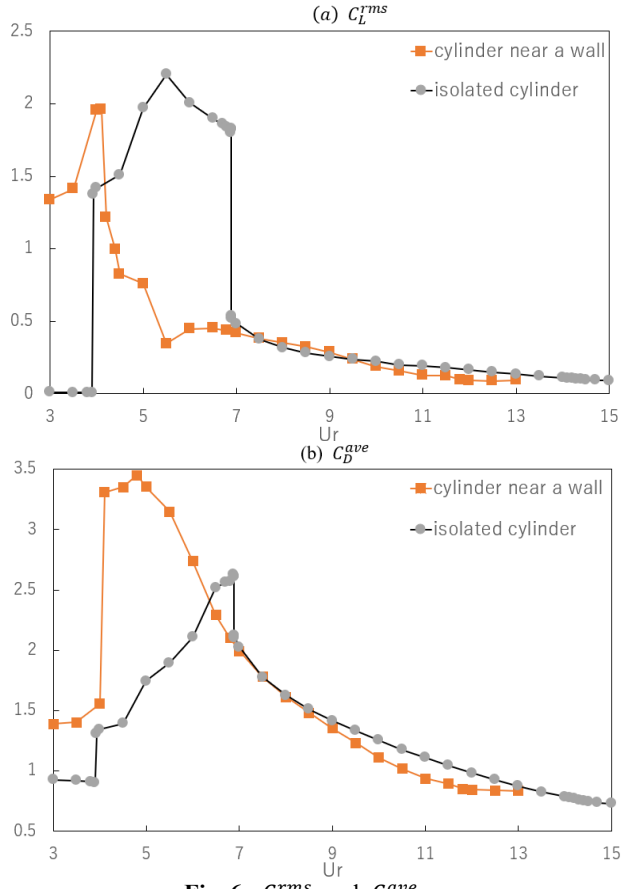

Fig. 6: C_L^{rms} and C_D^{ave}

4.2 Lift coefficient and drag coefficient

As shown in Fig. 6, lift coefficient and drag coefficient are compared. The root-mean-square of lift coefficient C_L^{rms} is illustrated in Fig. 6(a). At the initial branch ($U_r < 4$), the C_L^{rms} of the near-wall cylinder are bigger. At $U_r = 4.1$, two cylinders both go out the initial branch,

C_L^{rms} have a very sudden change like the corresponding vibration amplitudes curve. As Ur increases further, the C_L^{rms} of the isolated cylinder increase and then decrease rapidly at $U_r = 6.88$ which is same as the vibration amplitudes curve. In contrast, the C_L^{rms} of the cylinder near a wall decreases rapidly after it reaches the maximum at $U_r = 4.1$. Furthermore, for a near-wall cylinder, the average of lift coefficient is not 0 and the lift force direction is far from the wall.

As shown in Fig. 6(b), the relationship between average of drag coefficient C_D^{ave} and reduced velocity Ur is shown. The max C_D^{ave} of a near-wall cylinder is larger. Similar to C_L^{rms}, as Ur increases further, the C_D^{ave} of a near-wall cylinder will rise rapidly when $U_r = 4.1$, and then decreases.

At $7 < U_r < 15$, the curve of C_L^{rms} and C_D^{ave} are almost the same trend.

4.3 Frequency responses

The Fig. 7 illustrates the frequency ratio f/f_n with reduced velocity *Ur*. While *fs* is equal to or approximate to the cylinder natural frequency *fn*, lock-in occurs.

The near-wall cylinder goes into lock-in area at $U_r = 4.1$ while the isolated cylinder goes into lock-in area at $U_r = 6.88$. The vibration frequency of two cylinders both increases with Ur increases. The near-wall cylinder leaves the lock-in area at $U_r = 11.8$ while the isolated cylinder leaves the lock-in area at $U_r = 14$.

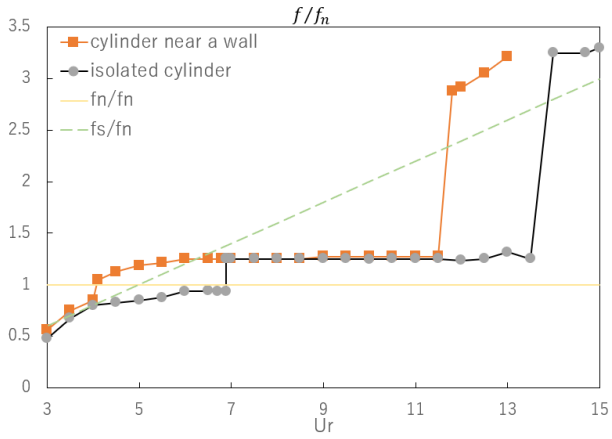

Fig. 7: Frequency ratio with reduced velocity.

4.4 Trajectory

As shown in Fig. 8, the track curve of vibration of the near-wall cylinder in X and Y direction is presented. As seen in numerous works of literature, the XY-trajectory of an isolated cylinder plots a shape of an eight. Tsahalis and Jones found that the track curves of vibration of the near-wall cylinder are an elliptical circle by experiments[5]. XY track curve of the cylinder near a wall in this article evolves from an irregular figure to a figure of eight, and then gradually becomes an enclosed elliptic circle as Ur rises.

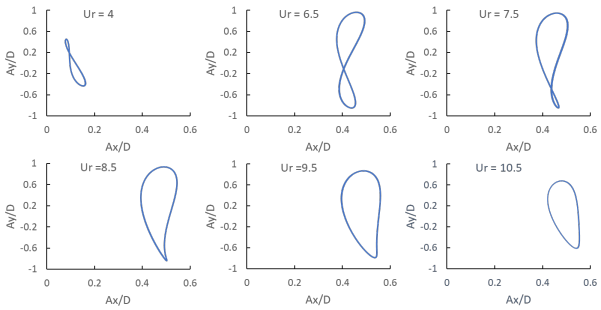

Fig. 8: XY-trajectory when a cylinder is near a wall.

4.5 Vorticity field

The vortex force and vorticity field are studied using five typical reduced velocities ($U_r = 4, 6, 8, 10, 12$). As shown in Fig. 9–13, the vorticity field and power spectrum analysis of lift coefficient (CL) of an isolated cylinder and a near-wall cylinder are illustrated.

The Fig. 9 shows the vorticity field and the power spectral analysis for lift coefficient of the isolated cylinder and the cylinder near a wall when $U_r = 4$ ($R_e = 2.1 \times 10^4$). There is only one peak in one vibration period in the power spectrum for two cylinders, and both are a typical 2S vortex mode observed from vorticity field. The vortex shedding from a wall interact with the vortex shedding from a cylinder, these vortex merge at the back of the cylinder. The lift coefficient amplitude of the isolated cylinder is smaller than that of the cylinder near the wall from the power spectrum.

The Fig. 10 shows the vorticity field and the power spectral analysis for lift coefficient of the isolated cylinder and the cylinder near a wall when $U_r = 6$ ($R_e = 3.1 \times 10^4$). For an isolated cylinder, two peaks can be seen from power spectrum, and the vortex mode where 2S mode transform into 2P mode can be observed from vorticity field. For the cylinder near a wall, three peaks can be observed from the power spectrum, and the vortex mode where 2P model transform into P + S mode can be observed from vorticity field. At $U_r = 6$, the transverse vibration amplitudes are large so that the wall boundary layer is disrupted by the vortex shedding from the cylinder, and which cause the wall boundary layer separate early. Then the vortex shedding closest to the wall from the cylinder merge with the wall boundary layer, and merge location is nearer cylinder than that at $U_r = 4$. The lift coefficient amplitude of the isolated cylinder is larger than that of the cylinder near the wall from the power spectrum.

The Fig. 11 shows the vorticity field and the power spectral analysis for lift coefficient of the isolated cylinder and the cylinder near a wall when $U_r = 8$ ($R_e = 4.2 \times 10^4$). For an isolated cylinder, two peaks can be seen from power spectrum, and a 2P vortex mode can be observed from vorticity field. For the cylinder near a wall, three peaks can be observed from the power spectrum, and the vortex mode where also 2P model transform into P + S mode can be observed from vorticity field. When $U_r = 8$, the isolated cylinder is already at lower branch, the lift

coefficient amplitude is very small compared to that at the upper branch. The lift coefficient amplitude of the isolated cylinder is almost equal to that of the cylinder near the wall from the power spectrum.

The Fig. 12 shows the vorticity field and the power spectral analysis for lift coefficient of the isolated cylinder and the cylinder near a wall when $U_r = 10$ ($R_e = 5.2 \times 10^4$). For an isolated cylinder, two peaks can be seen from the power spectrum, and a 2P vortex mode can be observed from vorticity field. For the cylinder near a wall, three peaks can be observed from the power spectrum, and the vortex mode where also 2P model transform into P + S mode can be observed from vorticity field. The lift coefficient amplitude of the isolated cylinder is a bit bigger than that of the cylinder near the wall from the power spectrum.

The Fig. 13 shows the vorticity field and the power spectral analysis for lift coefficient of the isolated cylinder and the cylinder near a wall when $U_r = 12$ ($R_e = 6.2 \times 10^4$). For an isolated cylinder, two peaks can be seen from power spectrum, and a 2P vortex mode can be observed from vorticity field. For the cylinder near a wall, a typical 2S vortex mode can be observed from vorticity field. When $U_r = 12$, the cylinder near a wall is at the desynchronization branch, compared to others Ur, only two peaks can be observed from the power spectrum, and the second frequency is dominant frequency. The lift coefficient amplitude is lesser than that of the isolated cylinder, however, frequency increases considerably as shown in Fig. 7.

5. Conclusion

The VIV dynamic response of the isolated cylinder and the cylinder near a wall are analyzed at reduced velocity $3 \leq U_r \leq 15$, corresponding Reynolds numbers $1.5 \times 10^4 \leq R_e \leq 7.8 \times 10^4$. The effects of the wall on VIV are studied. The main conclusions could be drawn as below:

(1) For an isolated cylinder, at $U_r = 6.88$, the max in-line amplitude is about 0.39D and the max transverse amplitude is about 1.46D. For a near-wall cylinder, the max transverse amplitude is about 0.99D at $U_r = 5.5$ and the max in-line amplitude is about 0.15D at $U_r = 4.5$.

(2) For an isolated cylinder, the max average drag coefficient is about 2.63, and the max lift coefficient root-mean-square is about 2.2. For a near-wall cylinder, the max average drag coefficient is about 3.45, and the max lift coefficient root-mean-square is about 1.96.

(3) For an isolated cylinder, as Ur increases, the 2S vortex model transform into 2P vortex mode. For a near-wall cylinder, as Ur increases, the 2S vortex model transform into 2P vortex mode, finally transform into P + S vortex mode at the lock-in area.

(4) The coupling responses between the cylinder and the wall are more complex. As a near-wall cylinder enters into lock-in area, vortex shedding from cylinder merge with those from the wall due to the large transverse amplitude of the cylinder, and these vortexes interact near the cylinder, which accelerate separation of wall boundary layer and alter the wake vortex structure.

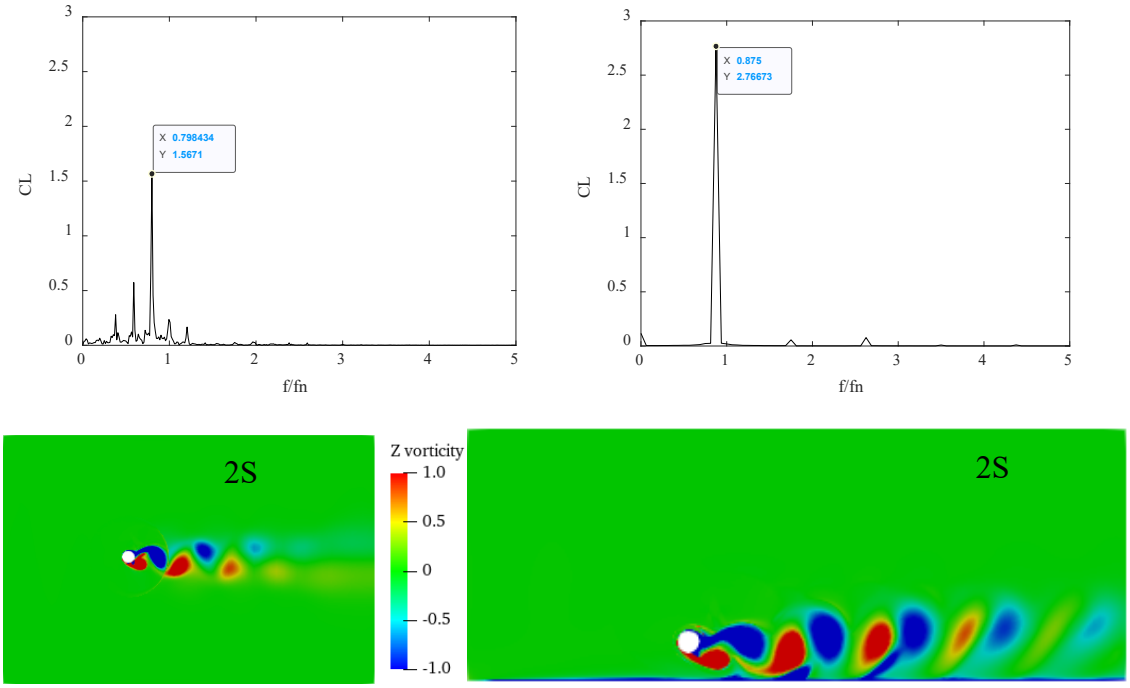

Fig. 9: Vorticity field and the power spectral analysis for lift coefficient of the isolated cylinder (left) and the cylinder near a wall (right) when Ur = 4 (Re = 2.1 × 10^4).

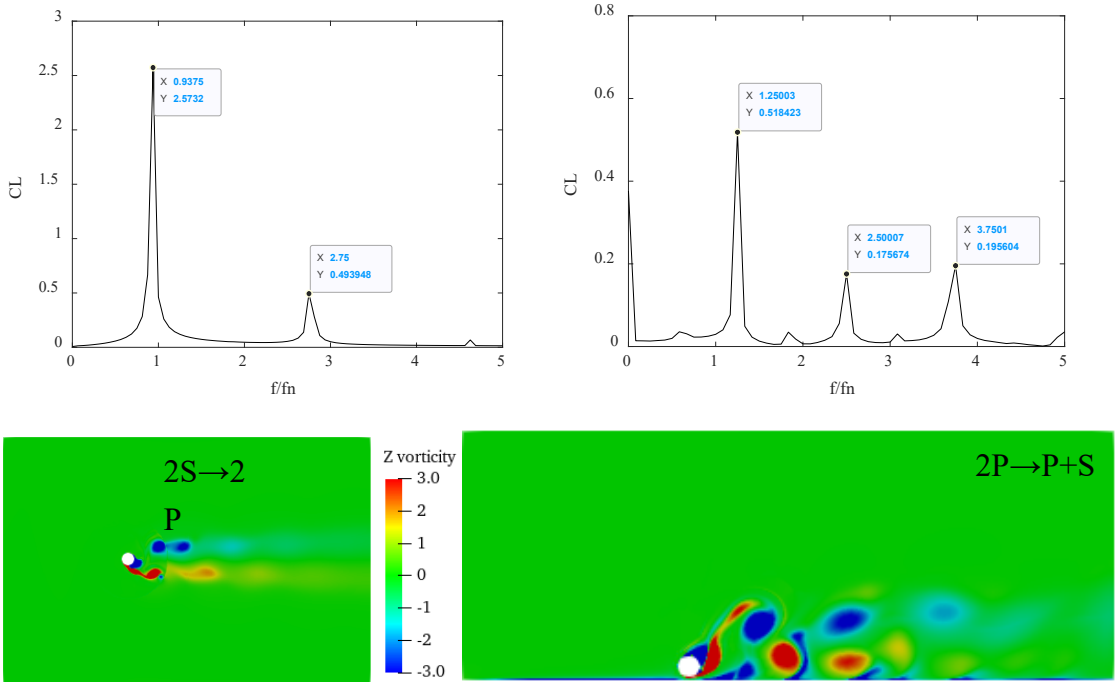

Fig. 10: Vorticity field and the power spectral analysis for lift coefficient of the isolated cylinder (left) and the cylinder near a wall (right) when Ur = 6 (Re = 3.1 × 10^4).

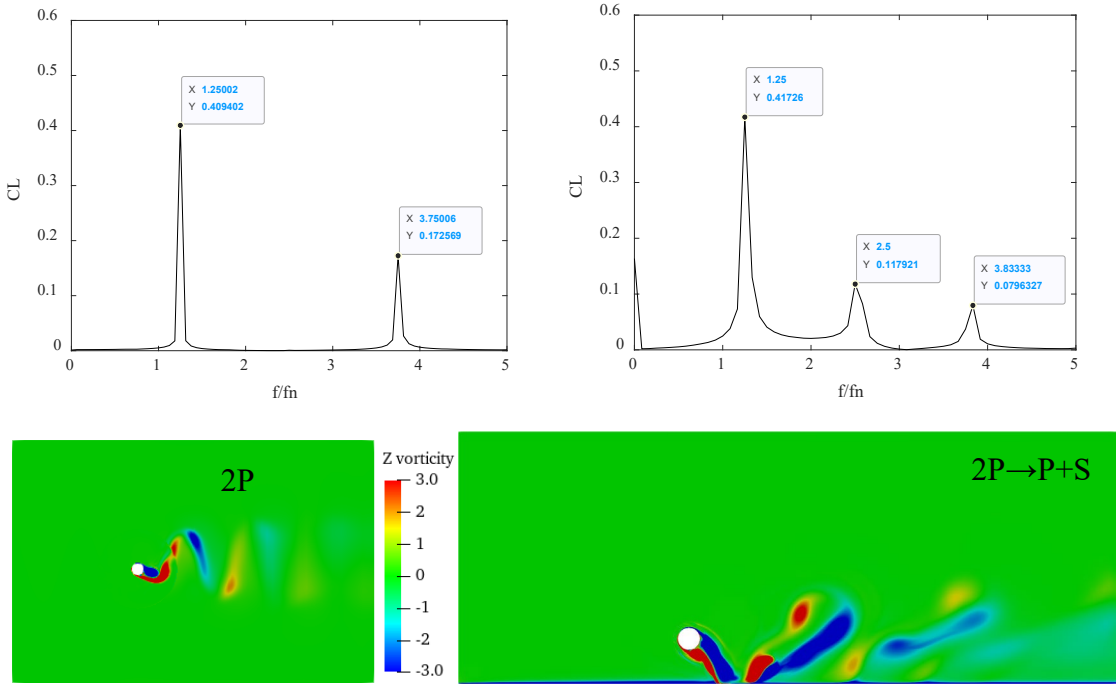

Fig. 11: Vorticity field and the power spectral analysis for lift coefficient of the isolated cylinder (left) and the cylinder near a wall (right) when Ur = 8 (Re = 4.2 × 10^4).

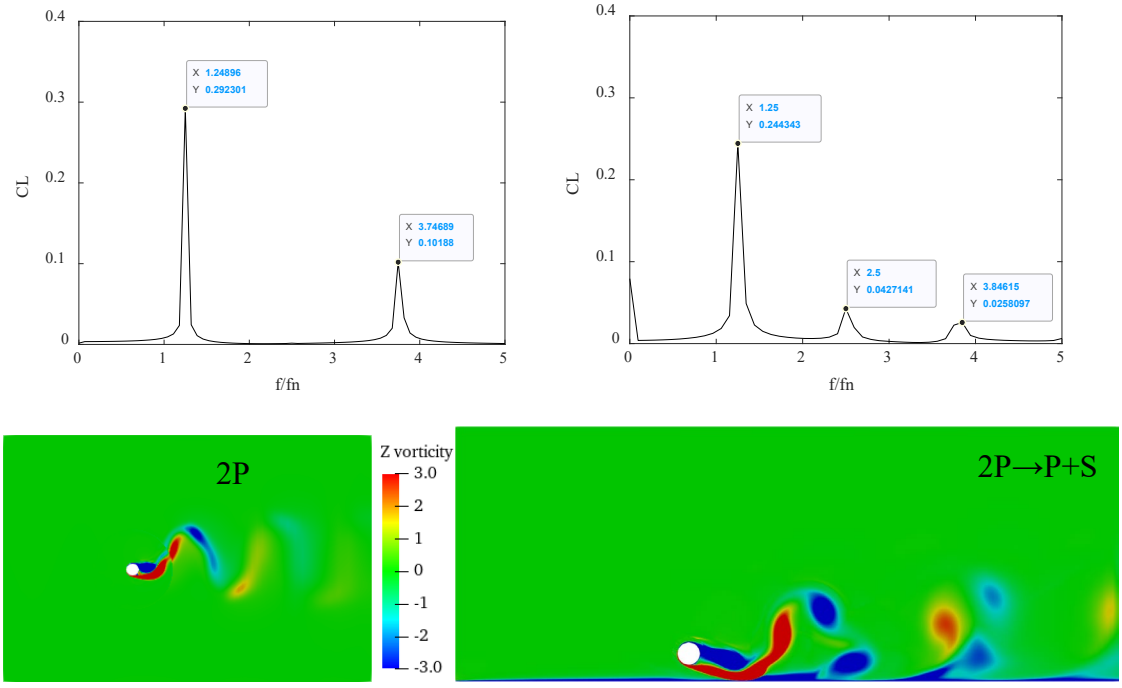

Fig. 12: Vorticity field and the power spectral analysis for lift coefficient of the isolated cylinder (left) and the cylinder near a wall (right) when Ur = 10 (Re = 5.2 × 10^4).

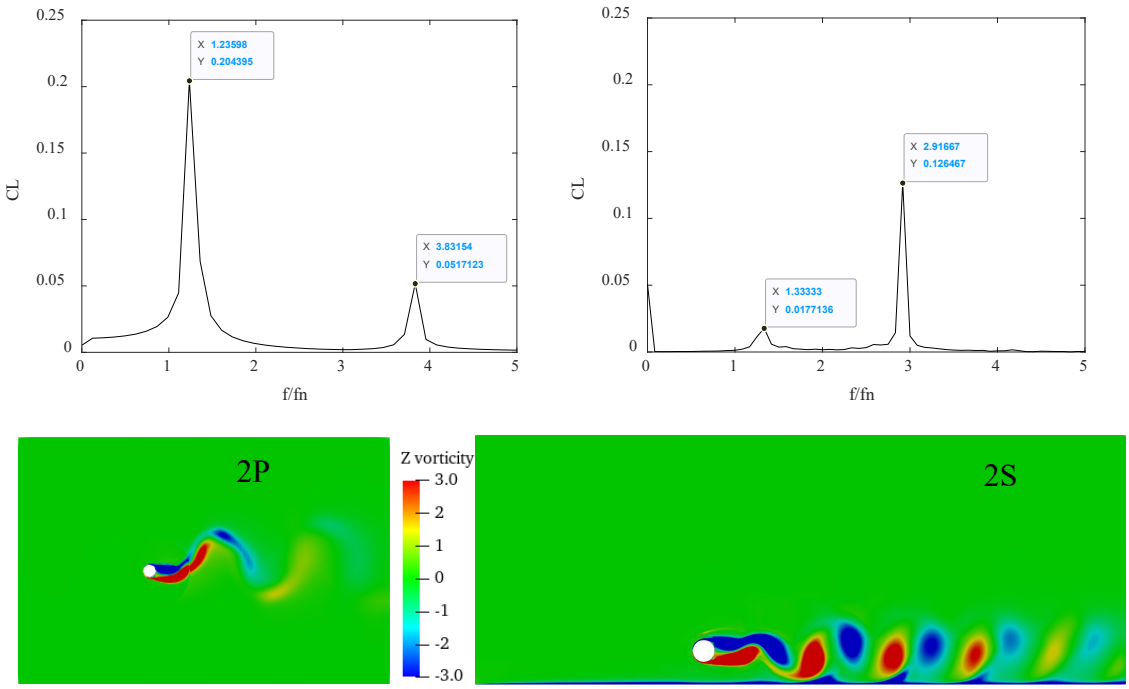

Fig. 13: Vorticity field and the power spectral analysis for lift coefficient of the isolated cylinder (left) and the cylinder near a wall (right) when Ur = 12 (Re = 6.2 × 10^4).

References

1) Barai M.K., and Saha B.B., "Energy Security and Sustainability in Japan," *Evergreen*, **2** (1) 49-56 (2015). doi:10.5109/1500427.

2) Moroga K., A. Nagata, and Y. Kuriyama, "State of implementation of environmental and energy policies adopted by the regional governments in Japan," *Evergreen*, **2** (2) 14-23 (2015). doi:10.5109/1544076.

3) Gima, H., and T. Yoshitake, "A Comparative Study of Energy Security in Okinawa Prefecture and the State of Hawaii," *Evergreen*, **3** (2) 36-44 (2016).

doi:10.5109/1800870.

4) Zhang Z, Ji C, and Xu D, "Temporal and spatial evolution of vortex shedding for flow around a cylinder close to a wall," *Ocean Engineering*, **228** (2021). doi:10.1016/j.oceaneng.2021.108964.
5) Tsahalis, D.T., "Vortex-Induced Vibrations of a Flexible Cylinder Near a Plane Boundary Exposed to Steady and Wave-Induced Currents." *ASME. J. Energy Resour. Technol*, **106** (2) 206–213 (1984). doi:10.1115/1.3231039.
6) Fredsoe, J., Sumer, B. M., Andersen, J., and Hansen, E. A.. "Transverse Vibrations of a Cylinder Very Close to a Plane Wall." *ASME. J. Offshore Mech. Arct. Eng. February*, **109** (1) 52–60 (1987). doi:10.1115/1.3256990.
7) Yang B, Gao F, and Wu Y, "Experimental study on flow induced vibration of a cylinder with two degrees of freedom near a rigid wall," *The Eighteenth International Offshore and Polar Engineering Conference, OnePetro*, **18** 469–473 (2008). doi:ISOPE-I-08-264.
8) Yang B., Gao F., Jeng D.S., and Wu Y., "Experimental study of vortex-induced vibrations of a cylinder near a rigid plane boundary in steady flow," *Acta Mechanica Sinica*, **25** (1) 51-63 (2009). doi:10.1007/s10409-008-0221-7.
9) Ming Z, and Liang C, "Numerical simulation of two-degree-of-freedom vortex-induced vibration of a circular cylinder close to a plane boundary,". *Journal of Fluids & Structures*, **27** (7) 1097-1110 (2011). doi:10.1016/j.jfluidstructs.2011.07.001.
10) Wang X.K., Hao Z, and Tan S.K., "Vortex-induced vibrations of a neutrally buoyant circular cylinder near a plane wall," *Journal of Fluids & Structures*, **39** 188-204 (2013). doi:10.1016/j.jfluidstructs.2013.02.012.
11) Tham D.M.Y., Gurugubelli P.S., Li Z., and Jaiman R.K., "Freely vibrating circular cylinder in the vicinity of a stationary wall," *Journal of Fluids and Structures*, **59** 103-128 (2015). doi:10.1016/j.jfluidstructs.2015.09.003.
12) Li Z., Yao W., Yang K., Jaiman R.K., and Khoo B.C., "On the vortex-induced oscillations of a freely vibrating cylinder in the vicinity of a stationary plane wall," *Journal of Fluids and Structures*, **65** 495-526 (2016). doi:10.1016/j.jfluidstructs.2016.07.001.
13) Chen L., Dong Y., and Wang Y., "Flow-induced vibration of a near-wall circular cylinder with a small gap ratio at low Reynolds numbers," *Journal of Fluids and Structures*, **103** (2021). doi:10.1016/j.jfluidstructs.2021.103247.
14) Chen Y., Fu S., Xu Y., and Fan D., "High order force components of a near-wall circular cylinder oscillating in transverse direction in a steady current," *Ocean engineering*, **74** 37-47 (2013). doi:10.1016/j.oceaneng.2013.09.009.
15) Chung M.H., "Transverse vortex-induced vibration of spring-supported circular cylinder translating near a plane wall," *European Journal of Mechanics - B/Fluids*, **55** (1) 88-103 (2016). doi:10.1016/j.euromechflu.2015.09.001.
16) de Oliveira Barbosa J.M., Qu Y., Metrikine A.V., and Lourens E.M., "Vortex-induced vibrations of a freely vibrating cylinder near a plane boundary: Experimental investigation and theoretical modelling," *Journal of Fluids and Structures*, **69** 382-401 (2017). doi:10.1016/j.jfluidstructs.2017.01.002.
17) Li Z., Jaiman R.K., and Khoo B.C., "Coupled dynamics of vortex-induced vibration and stationary wall at low Reynolds number," *Physics of Fluids*, **29** (9) (2017). doi:10.1063/1.4986410.
18) Munir A., Zhao M., Wu H., Ning D., and Lu L., "Numerical investigation of the effect of plane boundary on two-degree-of-freedom of vortex-induced vibration of a circular cylinder in oscillatory flow," *Ocean Engineering*, **148** 17-32 (2018). doi:10.1016/j.oceaneng.2017.11.022.
19) Chen W., Ji C., Xu D., and Williams J., "Two-degree-of-freedom vortex-induced vibrations of a circular cylinder in the vicinity of a stationary wall," *Journal of Fluids and Structures*, **91** (2019). doi:10.1016/j.jfluidstructs.2019.102728.
20) Daneshvar S., and Morton C., "On the vortex-induced vibration of a low mass ratio circular cylinder near a planar boundary," *Ocean Engineering*, **201** (2020). doi:10.1016/j.oceaneng.2020.107109.
21) Chen L.F., and Wu G.X., "Flow-induced transverse vibration of a circular cylinder close to a plane wall at small gap ratios," *Applied Ocean Research*, **103** (2020). doi:10.1016/j.apor.2020.102344.
22) Zhang Z., Ji C., Chen W., Hua Y., and Srinil N., "Influence of boundary layer thickness and gap ratios on three-dimensional flow characteristics around a circular cylinder in proximity to a bottom plane," *Ocean Engineering*, **226** (2021). doi:10.1016/j.oceaneng.2021.108858.
23) Pinguet R., Benoit M., Molin B., and Rezende F., "CFD analysis of added mass, damping and induced

flow of isolated and cylinder-mounted heave plates at various submergence depths using an overset mesh method," *Journal of Fluids and Structures*, **109** (2022). doi:10.1016/j.jfluidstructs.2021.103442.

24) Chen H, Qian L, Ma Z, Bai W, Li Y, Causon D., and Mingham C, "Application of an overset mesh based numerical wave tank for modelling realistic free-surface hydrodynamic problems," *Ocean Engineering*, **176** 97-117 (2019). doi:10.1016/j.oceaneng.2019.02.001.
25) Pinguet R, Kanner S, Benoit M and Molin B, "Validation of open-source overset mesh method using free-decay tests of floating offshore wind turbine," *The 30th International Ocean and Polar Engineering Conference. OnePetro*, (2020). doi:ISOPE-I-20-1179.
26) Menter F.R., "Two-equation eddy-viscosity turbulence models for engineering applications," *AIAA journal*, **32** (8) 1598-1605 (2015). doi:10.2514/3.12149.
27) Davidson L., "An introduction to turbulence models," Chalmers university of technology, (2015).
28) Naito H and Fukagata K, "Numerical simulation of flow around a circular cylinder having porous surface," *Physics of Fluids*, **24** (11) (2012). doi:10.1063/1.4767534.
29) Singh S.P., and Mittal S., "Vortex-induced oscillations at low Reynolds numbers: Hysteresis and vortex-shedding modes," *Journal of Fluids and Structures*, **20** (8) 1085-1104 (2005). doi:10.1016/j.jfluidstructs.2005.05.011.